JGR Space Physics

RESEARCH ARTICLE
10.1029/2021JA029729

Key Points:

- We have investigated the magnetosonic (MS) wave modulation by background plasma density using a 2-D general curvilinear particle-in-cell simulation
- MS waves can be locally excited by proton ring distribution in the low plasma density region, while no MS wave is generated in the high density region
- These MS waves are confined near the local source region since they are damped by the background cold plasma

Supporting Information:

Supporting Information may be found in the online version of this article.

Correspondence to:

J. Sun,
sun93@mail.ustc.edu.cn

Citation:

Sun, J., Lu, Q., Wang, X., Liu, X., Gao, X., & Yang, H. (2021). Modulation of magnetosonic waves by background plasma density in a dipole magnetic field: 2-D PIC simulation. *Journal of Geophysical Research: Space Physics*, *126*, e2021JA029729. https://doi.org/10.1029/2021JA029729

Received 29 JUN 2021
Accepted 12 OCT 2021

Modulation of Magnetosonic Waves by Background Plasma Density in a Dipole Magnetic Field: 2-D PIC Simulation

Jicheng Sun[1], Quanming Lu[2], Xueyi Wang[3], Xu Liu[4], Xinliang Gao[2], and Huigen Yang[1]

[1]MNR Key Laboratory for Polar Science, Polar Research Institute of China, Shanghai, China, [2]Department of Geophysics and Planetary Science, CAS Key Laboratory of Geospace Environment, University of Science and Technology of China, Hefei, China, [3]Department of Physics, Auburn University, Auburn, AL, USA, [4]Department of Physics, University of Texas at Dallas, Richardson, TX, USA

Abstract Recent satellite observations, combined with instability analyses, have shown that the background plasma density variation can modulate the magnetosonic (MS) waves by controlling the wave excitation. However, the detailed modulation process needs to be identified since the MS waves propagate nearly perpendicular to the background magnetic field. In this study, we investigate the MS wave modulation by background plasma density using a 2-D general curvilinear particle-in-cell simulation in the meridian plane of a dipole magnetic field. The simulation model consists of three plasma components: the background cold electrons and protons and ring distribution protons. We find that MS waves can be locally generated by ring distribution protons in the low plasma density region, while no MS wave is generated in the high density region. These MS waves are confined near the local source region since they are damped by the background cold plasma. The background protons gain more energy than background electrons, implying the plasmaspheric protons may dominate the modulation of MS waves. Moreover, we have also investigated the generation and propagation of MS waves in the plasmapause density structure. Our simulation results demonstrate that the background plasma density variation can modulate the MS waves and may play an important role in the spatial distribution of MS waves.

1. Introduction

Magnetosonic (MS) waves are an important electromagnetic emission occurring between the proton gyrofrequency and the lower hybrid frequency in the Earth's magnetosphere (Ma et al., 2013; Russell et al., 1970; Santolík et al., 2002). These waves propagate nearly perpendicular to the background magnetic field and typically exhibit a series of harmonics of the local proton gyrofrequency (e.g., Balikhin et al., 2015). Since MS waves are frequently observed within a few degrees of the geomagnetic equator, they are also known as equatorial noise in many literatures. In recent years, MS waves have come to the fore due to their potential roles in the energetic electron dynamic in the Van Allen radiation belt (Bortnik & Thorne, 2010; J. Li et al., 2014; Ni et al., 2017; Xiao et al., 2015). To be specific, using quasi-linear theory and test particle simulations, it is found that the MS waves can accelerate and scatter radiation belt electrons through Landau resonance (Horne et al., 2007), bounce resonance (Chen et al., 2015), and transit time effect (Bortnik & Thorne, 2010). Recently, using 2-D particle-in-cell (PIC) simulations, Sun, Chen, and Wang (2020) found that the wave normal angle (WNA) of MS waves can be significantly less than 89°. Those MS waves with relative small WNA can lead to a more efficient pitch angle and momentum diffusion of radiation belt electrons, potentially even more efficient than those by chorus waves. In addition, the PIC simulations (Chen et al., 2018; Sun et al., 2017) and satellite observation (Yuan et al., 2018) have shown that besides radiation belt electrons, MS waves can also interact with the plasmaspheric electron and protons, resulting in the energization of those background particles.

Satellite observations have shown that the MS waves in the magnetosphere are closely associated with the proton ring distribution at energies about dozens of keV (Boardsen et al., 1992; Meredith et al., 2008; Perraut et al., 1982). Theoretical analyses (Chen et al., 2010; Gary et al., 2010; Sun, Gao, Chen, et al., 2016) and PIC simulations (K. J. Liu et al., 2011; Sun, Gao, Lu, et al., 2016) further demonstrated that the MS waves can be excited by a proton ring distribution due to the positive gradient of phase space density around the

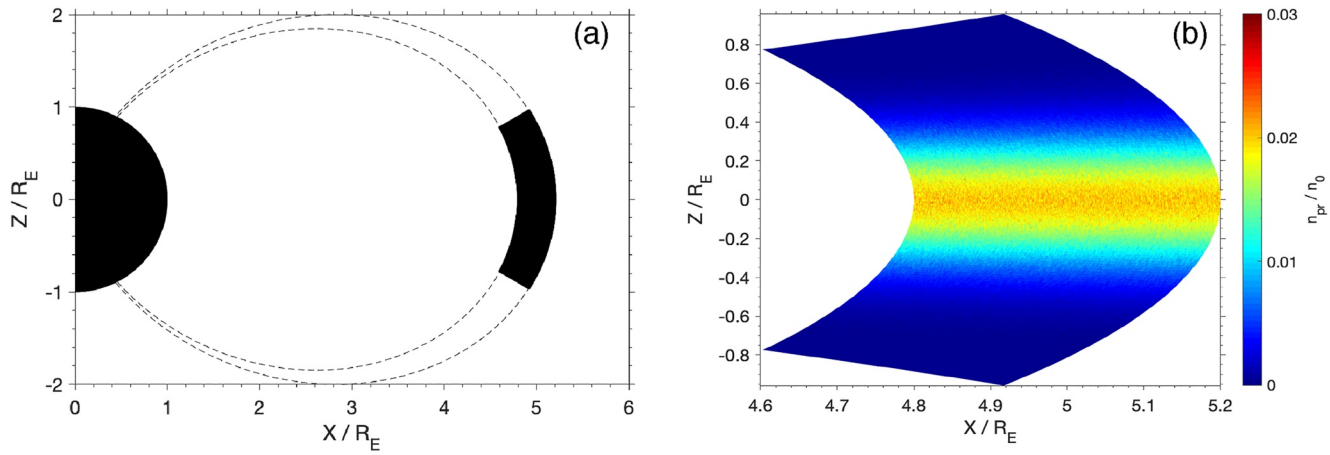

Figure 1. (a) The simulation domain shaded in black in Cartesian (x, z) coordinates on the meridian plane. The black dotted lines represent the magnetic field lines. (b) The initial number density of ring distribution protons inside the simulation domain.

local Alfven speed and have characteristics consistent with the observations: harmonics structures near the local proton gyrofrequency and nearly perpendicular propagation. Besides the harmonic structures, MS waves can exhibit other features, such as continuous spectra (Tsurutani et al., 2014) and rising-tone spectra (Boardsen et al., 2014; Fu et al., 2014). The former has been well explained by the linear theory (Chen et al., 2016; Sun, Gao, Chen, et al., 2016) and the latter has also been reproduced by the PIC simulation (Sun, Chen, Wang, et al., 2020).

Recently, the modulation of MS waves by background plasma density has been observed by the satellite (Yuan et al., 2017) because the background plasma density can control the wave growth rates and the MS waves can be only excited in the low density region. However, unlike whistler-mode and electromagnetic ion cyclotron (EMIC) waves that propagate parallel to the background magnetic field, the MS waves propagate nearly perpendicular to the background magnetic field. Thus, they may spread across the plasma density structure. In contrast to the satellite observation, no evidence of MS wave modulation by density variation is detected from the finite difference time domain (FDTD) simulation (as shown in Figure S1 in Supporting Information S1), since the FDTD simulation just considers the propagation effect of the electromagnetic waves (X. Liu et al., 2018). Thus, in this article, we use a 2-D general curvilinear PIC simulation to analyze whether the modulation of MS waves can occur in the Earth's magnetosphere. We investigate the generation and evolution of MS waves under different structures of background plasma density to achieve a realistic and consistent description of the modulation of MS waves. This article is organized as follows. Section 2 describes the 2-D general curvilinear PIC simulation model and initial parameters. Then, the simulation results are presented in Section 3. At last, conclusions and discussion are given in Section 4.

Table 1
Density Structures in r Direction for Different PIC Simulation Runs

Case number	Background plasma structure
1	Uniform density
2	Density dip of ratio 5
3	Plasmapause density ratio 10
4	Plasmapause density ratio 5

Note. PIC, particle-in-cell.

2. Simulation Model

The PIC simulation is a powerful tool to study the electromagnetic waves in the space plasma. In this article, we use a 2-D general curvilinear PIC simulation model to investigate the modulation of MS waves by the background plasma density in a dipole magnetic field. This simulation code has been successfully used to study the excitation of MS waves in a dipole magnetic field (Chen et al., 2018). The grid used in the simulation is based on a modified dipole coordinate system (r, q, s), in which r denotes L-shell, q varies along the dipole magnetic field, and s is pointed azimuthally. The detailed definition of this modified dipole coordinate system has been given in Chen et al. (2018). The computational domain of our study is illustrated by the black area of Figure 1a in the Cartesian

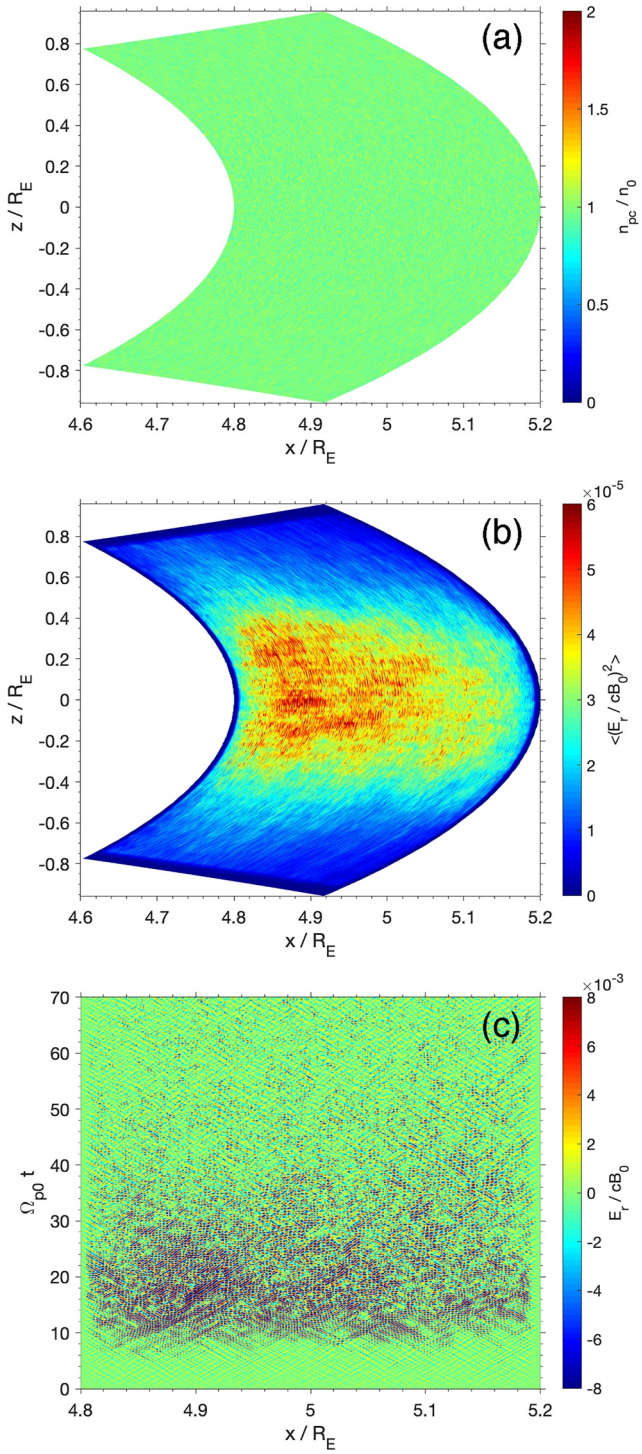

Figure 2. (a) The initial number density of background cold protons inside the simulation domain for Run 1. (b) The spatial distribution of the time-averaged fluctuating electric field E_r/cB_0 from $\Omega_{p0}t = 0$ to 70. (c) The temporal evolution of the radial component of fluctuating electric fields E_r/cB_0.

(x, z) coordinates in the meridian plane. The simulation domain consists of a 1,024 × 256 grid of evenly distributed bins in the ranges [4.8, 5.2] and [−0.15, 0.15] in the r and q directions, respectively. The value of $q = 0.15$ for the center r corresponds to $\lambda \approx 10°$ and $q = 0$ represents the magnetic equator.

For the initial condition, the plasma consists of three components: a ring distribution of hot protons, a Maxwellian distribution of cold electrons and protons. Hereafter, subscripts *pr*, *e*, and *pc* represent ring distribution protons, cold electrons, and cold protons, respectively. The ring distribution protons, as the free energy for MS waves, are distributed near the equator with number density n_{pr} (as shown in Figure 1b). The cold electrons are initialized to have number density n_0 and thermal speed v_{te}. The cold protons are assumed to have temperature equal to cold electron temperature and number density $n_{pc} = n_e - n_{pr}$ for the sake of charge neutrality. The detailed equation of the distribution of those three components has been described in Chen et al. (2018).

In our simulations, the magnetic field is normalized by the dipole magnetic field B_0 at $(r, q) = (L_0, 0)$, where L_0 is the center L shell of the simulation domain. The time and space are normalized to the inverse of electron gyrofrequency Ω_{e0} and the electron gyroradius v_{te}/Ω_{e0} (where v_{te} is the thermal speed of the cold electrons) at that location, respectively. The mass ratio of proton to electron is reduced such that $m_p/m_e = 100$, and the speed of light is also reduced to be $c = 20V_{A0}$, where $V_{A0} = B_0/\sqrt{\mu_0 n_0 m_p}$ is the Alfven speed at the central location of the simulation region. For the chosen values of the mass ratio, the proton gyrofrequency is $\Omega_{p0} = 0.01\Omega_{e0}$. The initial electron plasma beta at the position $(L_0, 0)$ is $\beta_e = 1.32 \times 10^{-4}$, then the thermal speed of cold electrons is $v_{te} = 0.08V_A$. The proton ring velocity is initialized as $V_R = V_A$, and the thermal speed of ring distribution protons is $0.1V_A$. The time step Δt is set as $\Omega_{e0}\Delta t = 0.05$. When translated to the physical setup, the central field line corresponds to $L_0 = 5$ and $B_0 = 248\,nT$, $n_0 = 10\,\mathrm{cm}^{-3}$. The cold electron and proton temperatures are $1eV$. The reflecting boundary conditions are assumed for particles, and absorbing boundary conditions are used for electromagnetic fields.

3. Simulation Results

With the 2-D general curvilinear PIC simulation model and the simulation setup described above, we examine the generation and evolution of MS waves under different structures of background plasma density in order to understand the modulation of MS waves in the Earth's magnetosphere. We consider three different types of background plasma density structures: uniform density, density dip, and plasmapause structure. The plasma density structures for the simulation runs are given in Table 1.

As a case for comparison, we first calculate the excitation and evolution of MS waves under uniform background density (Run 1). Figure 2a shows the initial spatial distribution of background cold protons for Run 1. Figure 2b shows the spatial distribution of the time-averaged fluctuating

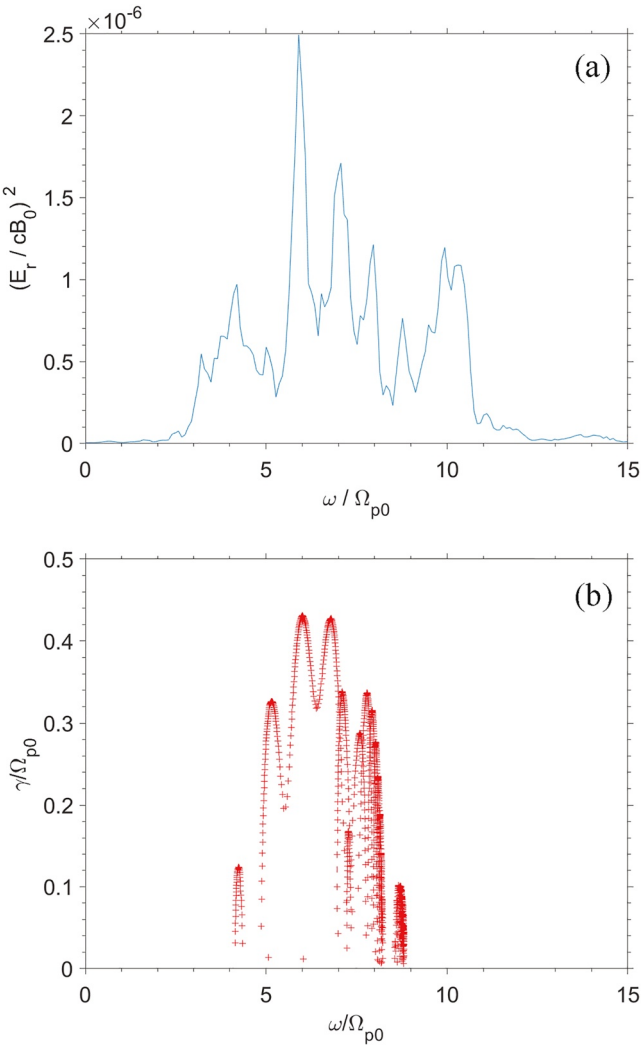

Figure 3. (a) The power spectrum density of fluctuating electric fields E_r/cB_0 at the central position $(r,q)=(L_0,0)$ over the time interval from $\Omega_{p0}t = 0$ to 60. (b) The normalized linear growth rate γ/Ω_{p0} versus the normalized wave frequency ω/Ω_{p0}, obtained from linear theory using the same parameters as the simulation.

electric field E_r from $\Omega_{p0}t$ =0 to 70. As can be seen from Figure 2b, in the x (r) direction, the waves can be excited in the whole range from r = 4.8 to 5.2 R_E, while in the z-direction, they are mainly generated near the equator, because the source region of the ring distribution is near the equator. Figure 2c displays the time evolution of the radial component of fluctuating electric fields E_r at the equator. As shown in Figure 2c, the waves start to be excited from about $\Omega_{p0}t$ = 5 and reach saturation at about $\Omega_{p0}t$ = 15. Due to the absorption boundary conditions we adopted, the intensity of waves gradually decreases after $\Omega_{p0}t$ = 40.

To further conform that the excited fluctuations are MS waves, we compare the simulation results against the linear theory. Figure 3a presents the power spectrum density of fluctuating electric fields E_r/cB_0 at the central position $(r,q)=(L_0,0)$ over the time interval from $\Omega_{p0}t$ = 0 to 60 for Run 1. Figure 3b shows the normalized linear growth rate γ/Ω_{p0} obtained from linear theory using the same parameters as the simulation. The power spectral density shows discrete peaks at harmonic frequencies from 4 to 10Ω_{p0}. Most of these discrete peaks are consistent with the growth rate profile predicted from the linear theory, except for the peak at 10Ω_{p0}. The peak at 10Ω_{p0} obtained from the simulation, inconsistent with the linear theory, may be due to the propagation from the off-equator region. Based on the wave spectrum of the simulation and the comparison with the linear theory, we can conclude that the excited fluctuating electromagnetic fields in the simulations are indeed MS waves generated by the proton ring distribution.

Figure 4a shows the initial spatial distribution of background protons for Run 2. In this case, we construct a density dip in the r direction and the equatorial distribution of background protons $n_{pc,eq}(r)$ adopts the following form:

$$n_{pc,eq} = n_0\left(5 - 4\exp\left(-\frac{\left(r-L_0\right)^2}{\left(0.1\Delta L\right)^2}\right)\right), \quad (1)$$

where ΔL denotes the simulation length in the r direction. Figure 4b displays the spatial distribution of the time-averaged fluctuating electric field E_r from $\Omega_{p0}t$ = 0 to 70. It can be seen from the figure that the MS waves mainly appear in the range of x = 4.95 to 5.05 R_E and z = –0.2 to 0.2 R_E. This is because the MS waves can only be excited by the ring distribution proton in the low density region, at which the MS waves have the positive growth rate. Chen et al. (2010) have shown that when ring distribution protons are injected into the inner magnetosphere, MS waves can be excited at the region of V_R/V_A <~2. In our simulation, V_R/V_A is larger than 2 in the high density region and thus the MS waves have the negative growth rate in that region. The simulation results are consistent with satellite observations that MS waves occur only in the region of low plasma density (Yuan et al., 2017). The time evolution of the radial component of fluctuating electric fields E_r at the equator is shown in Figure 4c. We can also find that more intense fields occur mainly in the central region of the simulation (x = 4.95 to 5.05 R_E), indicating the MS waves are confined in the low density regions at the equator.

To analyze why MS waves are confined in the low density regions, we examine the temporal and spatial evolution of kinetic energy for different species of particles in Run 2. Since the particles can easily bounce along the magnetic field lines, the particles heated by the MS waves may leave the equatorial source region. Thus, we need to average the particle energy along the direction of the magnetic field line. The parallel and perpendicular temperature of particles is calculated as

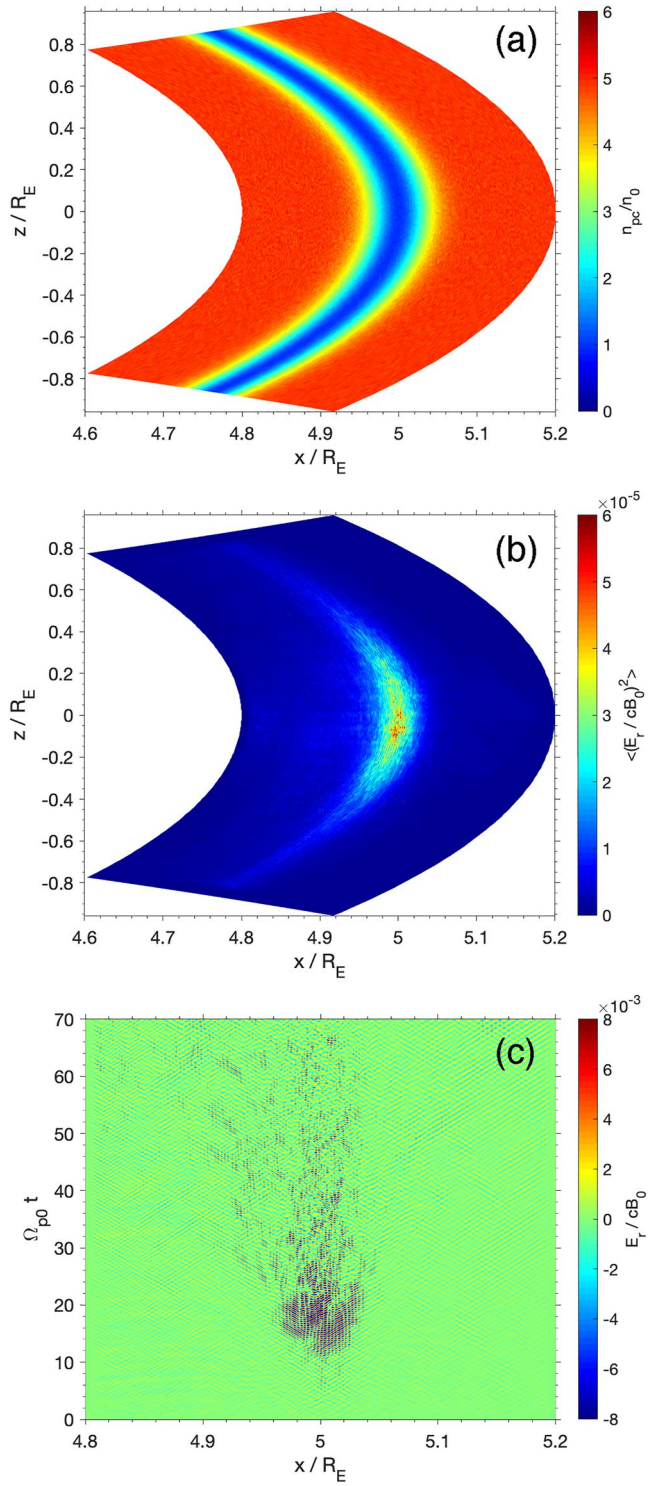

Figure 4. The same format as Figure 2 except for Run 2.

$$E_{j\parallel} = m_j\langle v_{jq}{}^2\rangle, \tag{2}$$

and

$$E_{j\perp} = m_j\langle v_{jr}{}^2 + v_{js}{}^2\rangle, \tag{3}$$

where the angle brackets denote an average over particles of species j inside the cells at the same *L-shell*. Figure 5 shows the perpendicular kinetic energy of cold protons (Figure 5a), the parallel kinetic energy of cold protons (Figure 5b), the perpendicular kinetic energy of cold electrons (Figure 5c), and the parallel kinetic energy of cold electrons (Figure 5d). All of the kinetic energy is normalized by the initial electron energy $E_{e0} = m_e v_{te}^2$. As can be seen from the figure, with the excitation of MS waves, the background cold protons and electrons are heated in the perpendicular direction from $\Omega_{p0}t = 20$. Sun et al. (2017) have suggested that the background plasma can be heated by the MS waves and this is consistent with the present simulation result. Compared with the MS waves gradually weakened from $\Omega_{p0}t = 20$ (Figure 4c), we can find that the MS waves are dissipated by the background cold plasma. Thus, we conclude that the heating of the background plasma by MS waves in turn leads to the dissipation of MS waves. Besides, it can be found that the background protons gain more energy than background electrons, implying the plasmaspheric protons may dominate the dissipation of MS waves in the magnetosphere.

We further investigate the effect of plasmapause on the propagation of the MS waves. Figure 6a shows the initial spatial distribution of background protons for Run 3 (density ratio 10). The equatorial distribution $n_{pc,eq}(r)$ for Run 3 adopts the form of

$$n_{pc}/n_0 = 5.5 - 4.5\tanh\left(-\frac{\mathrm{r} - L_0 - l}{\delta}\right), \tag{4}$$

where $l = \Delta L/80$ and $\delta = \Delta L/10$. Figure 6b shows the spatial distribution of the time-averaged fluctuating electric field E_r from omega $t = 0$ to 70, and Figure 6c shows the time evolution of the radial component of fluctuating electric fields E_r at the equator. Figures 6d–6f show the same format as Figures 6a–6c except for Run 4 (density ratio 5). The equatorial distribution $n_{pc,eq}(r)$ for Run 4 adopts the form of

$$n_{pc}/n_0 = 3 - 2\tanh\left(-\frac{\mathrm{r} - L_0 - l}{\delta}\right), \tag{5}$$

where $l = \Delta L/80$ and $\delta = \Delta L/10$. By comparing Figures 6c and 6f, it can be seen that when the density ratio is low (density ratio 5), the MS waves can propagate to a deeper distance, and when the density ratio is high, the MS waves can hardly pass through the plasmapause. Regarding to the effects of the plasmapause on the radial propagation of MS waves, Yu et al. (2021) also investigated this effect using an analytical approach

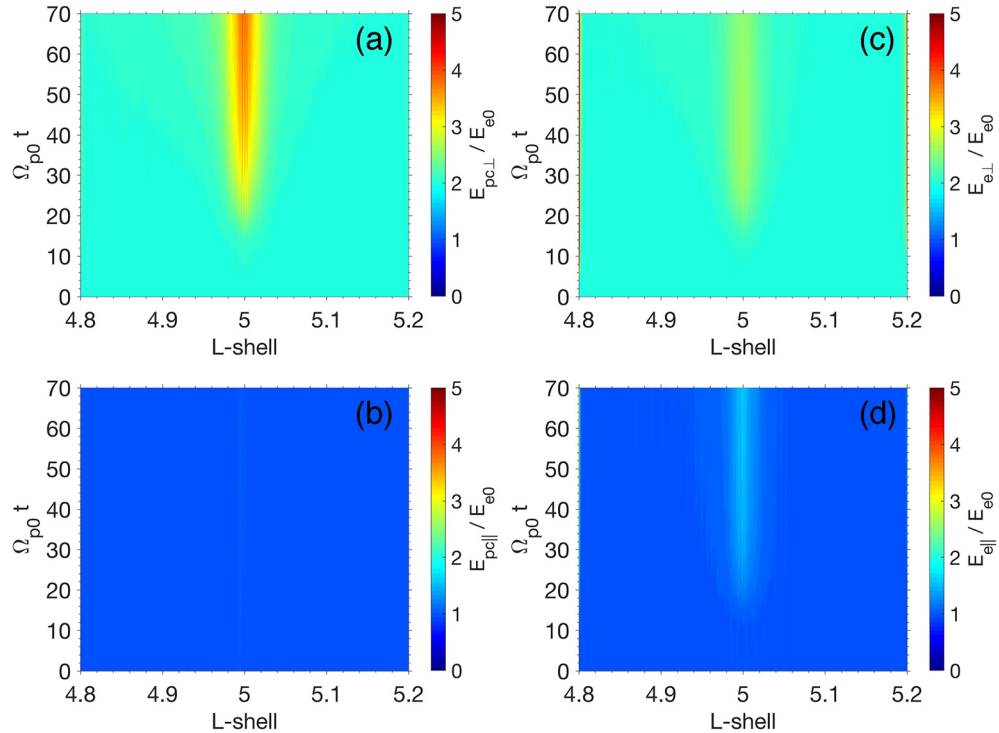

Figure 5. The temporal and spatial evolution of (a) the perpendicular kinetic energy of cold protons, (b) the parallel kinetic energy of cold protons, (c) the perpendicular kinetic energy of cold electrons, and (d) the parallel kinetic energy of cold electrons.

and they found when the width of the plasmapause boundary layer is narrow in comparison with the wavelength of MS waves, a significant part of waves will be reflected. While the plasmapause boundary layer is much larger than the wavelength of MS waves and there is almost no reflection in our simulation.

4. Conclusions and Discussion

In this article, by performing 2-D PIC simulations, we have studied the modulation of MS waves by the background plasma density in the meridian plane of a dipole magnetic field. Our study found that MS waves can be locally generated by ring distribution protons in the low plasma density region, while there are no MS waves generated in the high plasma density region. These waves are confined near the low density region at which the growth rate of waves is positive, since the waves are subject to damping from the background cold plasma. The cold protons gain more energy than cold electrons, implying the plasmaspheric protons may dominate the modulation of MS waves. Moreover, the generation and propagation of MS waves in the plasmapause density structure have also been investigated. Our simulation results demonstrate that the MS waves can be modulated by the background plasma density in the dipole magnetic field. This modulation may play an important role in the spatial distribution of the MS waves in the magnetosphere.

Modulation of electromagnetic waves by the background plasma density is a common phenomenon in the magnetosphere, such as the whistlers (W. Li et al., 2011), the EMIC (S. Liu et al., 2019), and the MS waves (Němec et al., 2020; Yuan et al., 2017). Different from the whistle and EMIC waves that propagate parallel to the background magnetic field, the MS waves propagate nearly perpendicular to the background magnetic field. Thus, a more detailed analysis of the modulation of MS waves is required. Min et al. (2019) have investigated the propagation of MS waves in the equatorial plane and they found refraction at the plasmapause can redirect the propagation of MS waves. In this study, we investigate the behavior of MS waves under different structures of background plasma density in the meridian plane. Our PIC simulation on the meridian plane shows that the MS waves cannot cross the density gradient far away from the source region and they are modulated by the plasma density because of the dissipation of the waves by the background

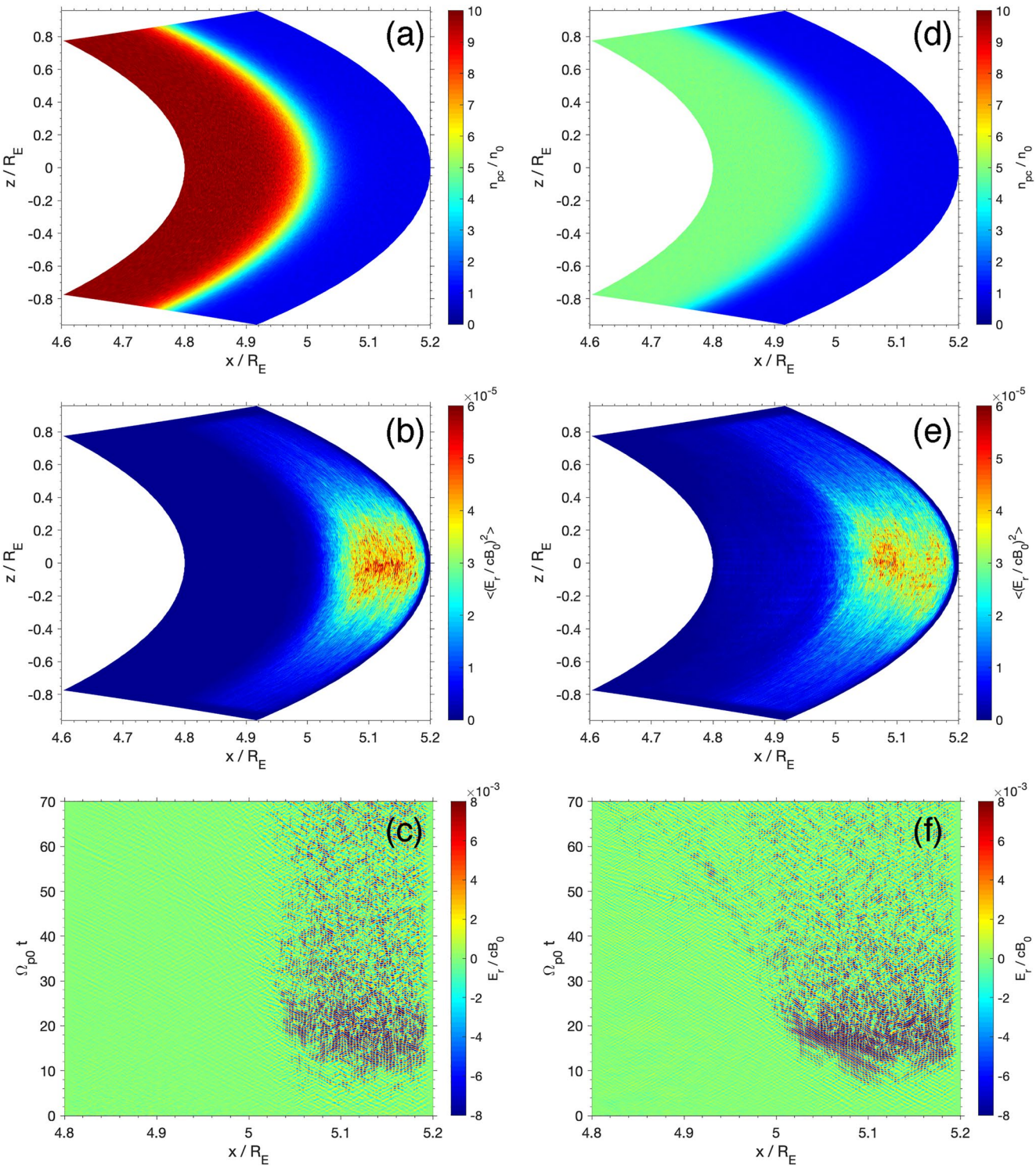

Figure 6. The same format as Figure 2 except for Run 3 (left column) and Run 4 (right column).

plasma. The MS waves in the Earth's magnetosphere cannot strictly propagate in the meridional plane or the equatorial plane. So which mechanism dominates the modulation of the MS waves still needs to be analyzed through 3-D simulation. Therefore, the 3-D PIC simulation of MS wave excitation in the dipole magnetic field will be investigated in the future.

Data Availability Statement

The simulation data which is used to plot the figures all can be downloaded from https://doi.org/10.5281/zenodo.5040250.

Acknowledgment
This work was supported by the National Natural Science Foundation of China (grant numbers 41831072).

References

Balikhin, M. A., Shprits, Y. Y., Walker, S. N., Chen, L., Cornilleau-Wehrlin, N., Dandouras, I., et al. (2015). Observations of discrete harmonics emerging from equatorial noise. *Nature Communications*, *6*, 7703. https://doi.org/10.1038/ncomms8703

Boardsen, S. A., Gallagher, D. L., Gurnett, D. A., Peterson, W. K., & Green, J. L. (1992). Funnel-shaped, low-frequency equatorial waves, *Journal of Geophysical Research*, *97*, 14967–14976. https://doi.org/10.1029/92JA00827

Boardsen, S. A., Hospodarsky, G. B., Kletzing, C. A., Pfaff, R. F., Kurth, W. S., Wygant, J. R., & MacDonald, E. A. (2014). Van Allen probe observations of periodic rising frequencies of the fast magnetosonic mode. *Geophysical Research Letters*, *41*, 8161–8168. https://doi.org/10.1002/2014GL062020

Bortnik, J., & Thorne, R. M. (2010). Transit time scattering of energetic electrons due to equatorially confined magnetosonic waves. *Journal of Geophysical Research*, *115*(A7), A07213. https://doi.org/10.1029/2010JA015283

Chen, L., Maldonado, A., Bortnik, J., Thorne, R. M., Li, J., Dai, L., & Zhan, X. (2015). Nonlinear bounce resonances between magnetosonic waves and equatorially mirroring electrons. *Journal of Geophysical Research: Space Physics*, *120*, 6514–6527. https://doi.org/10.1002/2015JA021174

Chen, L., Sun, J., Lu, Q., Gao, X., Xia, Z., & Zhima, Z. (2016). Generation of magnetosonic waves over a continuous spectrum. *Journal of Geophysical Research: Space Physics*, *121*, 1137–1147. https://doi.org/10.1002/2015JA022089

Chen, L., Sun, J., Lu, Q., Wang, X., Gao, X., Wang, D., & Wang, S. (2018). Two-dimensional particle-in-cell simulation of magnetosonic wave excitation in a dipole magnetic field. *Geophysical Research Letters*, *45*, 8712–8720. https://doi.org/10.1029/2018GL079067

Chen, L., Thorne, R. M., Jordanova, V. K., & Horne, R. B. (2010). Global simulation of magnetosonic wave instability in the storm time magnetosphere. *Journal of Geophysical Research*, *115*. https://doi.org/10.1029/2010JA015707

Fu, H. S., Cao, J. B., Zhima, Z., Khotyaintsev, Y. V., Angelopoulos, V., Santolik, O., et al. (2014). First observation of rising-tone magnetosonic waves. *Geophysical Research Letters*, *41*, 7419–7426. https://doi.org/10.1002/2014GL061867

Gary, S. P., Liu, K., Winske, D., & Denton, R. E. (2010). Ion Bernstein instability in the terrestrial magnetosphere: Linear dispersion theory. *Journal of Geophysical Research*, *115*. https://doi.org/10.1029/2010JA015965

Horne, R. B., Thorne, R. M., Glauert, S. A., Meredith, N. P., Pokhotelov, D., & Santolik, O. (2007). Electron acceleration in the Van Allen radiation belts by fast magnetosonic waves. *Geophysical Research Letters*, *34*, L17107. https://doi.org/10.1029/2007GL030267

Li, J., Ni, B., Xie, L., Pu, Z., Bortnik, J., Thorne, R. M., et al. (2014). Interactions between magnetosonic waves and radiation belt electrons: Comparisons of quasi-linear calculations with test particle simulations. *Geophysical Research Letters*, *41*, 4828–4834. https://doi.org/10.1002/2014GL060461

Li, W., Bortnik, J., Thorne, R. M., Nishimura, Y., Angelopoulos, V., & Chen, L. (2011). Modulation of whistler mode chorus waves: 2. Role of density variations. *Journal of Geophysical Research*, *116*, A06206. https://doi.org/10.1029/2010JA016313

Liu, K. J., Gary, S. P., & Winske, D. (2011). Excitation of magnetosonic waves in the terrestrial magnetosphere: Particle-in-cell simulations. *Journal of Geophysical Research*, *116*, A07212. https://doi.org/10.1029/2010JA016372

Liu, S., Xia, Z., Chen, L., Liu, Y., Liao, Z., & Zhu, H. (2019). Magnetospheric Multiscale Observation of quasiperiodic EMIC waves associated with enhanced solar wind pressure. *Geophysical Research Letters*, *46*, 7096–7104. https://doi.org/10.1029/2019GL083421

Liu, X., Chen, L., Yang, L., Xia, Z., & Malaspina, D. M. (2018). One-dimensional full wave simulation of equatorial magnetosonic wave propagation in an inhomogeneous magnetosphere. *Journal of Geophysical Research: Space Physics*, *123*, 587–599. https://doi.org/10.1002/2017JA024336

Ma, Q. L., Li, W., Thorne, R. M., & Angelopoulos, V. (2013). Global distribution of equatorial magnetosonic waves observed by THEMIS. *Geophysical Research Letters*, *40*(10), 1895–1901. https://doi.org/10.1002/grl.50434

Meredith, N. P., Horne, R. B., & Anderson, R. R. (2008). Survey of magnetosonic waves and proton ring distributions in the Earth's inner magnetosphere. *Journal of Geophysical Research*, *113*, A06213. https://doi.org/10.1029/2007JA012975

Min, K., Ne˘mec, F., Liu, K., Denton, R. E., & Boardsen, S. A. (2019). Equatorial propagation of the magnetosonic mode across the plasmapause: 2-D PIC simulations. *Journal of Geophysical Research: Space Physics*, *124*, 4424–4444. https://doi.org/10.1029/2019ja026567

Němec, F., Tomori, A., Santolík, O., Boardsen, S. A., Hospodarsky, G. B., Kurth, W. S., et al. (2020). Fine harmonic structure of equatorial noise with a quasiperiodic modulation. *Journal of Geophysical Research: Space Physics*, *125*, e2019JA027509. https://doi.org/10.1029/2019JA027509

Ni, B., Hua, M., Zhou, R. X., Yi, J., & Fu, S. (2017). Competition between outer zone electron scattering by plasmaspheric hiss and magnetosonic waves. *Geophysical Research Letters*, *44*(8), 3465–3474. https://doi.org/10.1002/2017GL072989

Perraut, S., Roux, A., Robert, P., Gendrin, R., Sauvaud, J., Bosqued, J., et al. (1982). A systematic study of ULF waves above F/H+ from GEOS 1 and 2 measurements and their relationships with proton ring distributions. *Journal of Geophysical Research*, *87*, 6219–6236. https://doi.org/10.1029/JA087iA08p06219

Russell, C. T., Holzer, R. E., & Smith, E. J. (1970). OGO 3 observations of ELF noise in the magnetosphere: 2. The nature of the equatorial noise. *Journal of Geophysical Research*, *75*(4), 755–768. https://doi.org/10.1029/JA075i004p00755

Santolik, O., Pickett, J. S., Gurnett, D. A., Maksimovic, M., & Cornilleau-Wehrlin, N. (2002). Spatiotemporal variability and propagation of equatorial noise observed by Cluster. *Journal of Geophysical Research*, *107*, 1495. https://doi.org/10.1029/2001ja009159

Sun, J., Chen, L., & Wang, X. (2020). Wave normal angle distribution of magnetosonic waves in the Earth's magnetosphere: 2D PIC simulation. *Journal of Geophysical Research: Space Physics*, *125*, e2020JA028012. https://doi.org/10.1029/2020ja028012

Sun, J., Chen, L., Wang, X., Boardsen, S., Lin, Y., & Xia, Z. (2020). Particle-in-cell simulation of rising-tone magnetosonic waves. *Geophysical Research Letters*, *47*, e2020GL089671. https://doi.org/10.1029/2020GL089671

Sun, J., Gao, X., Chen, L., Lu, Q., Tao, X., & Wang, S. (2016). A parametric study for the generation of ion Bernstein modes from a discrete spectrum to a continuous one in the inner magnetosphere. I. Linear theory. *Physics of Plasmas*, *23*(2), 022901. https://doi.org/10.1063/1.4941283

Sun, J., Gao, X., Lu, Q., Chen, L., Liu, X., Wang, X., et al. (2017). Spectral properties and associated plasma energization by magnetosonic waves in the Earth's magnetosphere: Particle-in-cell simulations. *Journal of Geophysical Research: Space Physics*, *122*, 5377–5390. https://doi.org/10.1002/2017JA024027

Sun, J., Gao, X., Lu, Q., Chen, L., Tao, X., & Wang, S. (2016). A parametric study for the generation of ion Bernstein modes from a discrete spectrum to a continuous one in the inner magnetosphere. II. Particle-in-cell simulations. *Physics of Plasmas*, *23*(2), 022902. https://doi.org/10.1063/1.4941284

Tsurutani, B. T., Falkowski, B. J., Pickett, J. S., Verkhoglyadova, O. P., Santolik, O., & Lakhina, G. S. (2014). Extremely intense ELF magnetosonic waves: A survey of polar observations. *Journal of Geophysical Research: Space Physics*, *119*, 964–977. https://doi.org/10.1002/2013JA019284

Xiao, F. L., Yang, C., Su, Z. P., Zhou, Q. H., He, Z. G., He, Y. H., et al. (2015). Wave-driven butterfly distribution of Van Allen belt relativistic electrons. *Nature Communications*, *6*(1), 8590. https://doi.org/10.1038/ncomms9590

Yu, X., Yuan, Z., Ouyang, Z., & Yao, F. (2021). Effects of the plasmapause on the radial propagation of fast magnetosonic waves: An analytical approach. *Journal of Geophysical Research: Space Physics*, *126*, e2020JA028330. https://doi.org/10.1029/2020ja028330

Yuan, Z., Yu, X., Huang, S., Qiao, Z., Yao, F., & Funsten, H. O. (2018). Cold ion heating by magnetosonic waves in a density cavity of the plasmasphere. *Journal of Geophysical Research: Space Physics*, *123*, 1242–1250. https://doi.org/10.1002/2017JA024919

Yuan, Z., Yu, X., Huang, S., Wang, D., & Funsten, H. O. (2017). In situ observations of magnetosonic waves modulated by background plasma density. *Geophysical Research Letters*, *44*, 7628–7633. https://doi.org/10.1002/2017GL074681